General Base-Catalyzed Rates of Dissociation of Hemiacetals and the Hydrate of Acetaldehyde Conform to a Reaction Surface Based on the Marcus Function

D. L. Leussing

Department of Chemistry, The Ohio State University, Columbus, Ohio 43210

Received June 19, 1989

Rate constants earlier reported for the general base-catalyzed dissociation of hemiacetals and the hydrate of acetaldehyde have been examined in the context of a reaction surface that has been derived on the basis of the Marcus equation. With the thermodynamic stabilities of the species located at the corners of the reaction surface, rate constants for the dissociation of six hemiacetals catalyzed by eight bases ranging in basicity from H_2O to OH^- are quite satisfactorily reproduced with a two-parameter function for the intrinsic barrier, $\Delta G_0^{\ddagger} = 3.5\ (3) + (0.36\ (3))pK_{ROH}$ kcal mol^{-1}. Rate constants for dehydration are reproduced by a single value of the intrinsic barrier, 10.4 (2) kcal mol^{-1}. Direct nucleophilic attack of OH^- on the keto carbon of acetaldehyde exhibits an intrinsic barrier of 11.3 kcal mol^{-1}. The nature of the dependency of the intrinsic barrier on the nucleophile basicity suggests that nucleophilic desolvation comprises a major contribution to the reaction barrier. A linear relationship exists between the calculated coordinates of the transition state and the Brønsted coefficients, β and β_{lg}. However, the equation that relates β_{lg} to the reaction coordinates also contains a constant that originates from the dependence of $\Delta G_0^{\ddagger}$ on pK_{ROH}. In general, the influence of such terms can introduce errors in estimations from the Brønsted parameters of transition-state locations. In the earlier work the kinetic results were interpreted assuming the reaction surface resembles a hyperbolic paraboloid in the vicinity of the transition state. The failure of this earlier model to account for rates of OH^--catalyzed hemiacetal dissociation had been attributed to a change in mechanism from class *n* with the weaker base catalysts to direct uncatalyzed cleavage of RO^- from the hemiacetal.[16] The reaction surface examined in this work quite clearly shows this mechanistic change and provides close estimates of the rate constants for both mechanisms.

Over the years we have had a long-standing interest in labile metal ion–general base- or general acid-cocatalyzed reactions of carbonyl compounds. In searching for an explanation for the strong correlation between metal-ion-induced rate enhancements observed in various types of reactions, we have found[1-4] that the Marcus equation,[5] (1), quantitatively accounts for a number of the results.

$$\Delta G^{\ddagger} = \Delta G_0^{\ddagger} + \Delta G^{\circ}/2 + (\Delta G^{\circ})^2/16\Delta G_0^{\ddagger} \qquad (1)$$

The Marcus equation relates the reaction rate constant to a kinetic parameter $\Delta G_0^{\ddagger}$, which is known as the intrinsic barrier, and the thermodynamic free energy change across the rate-limiting step. Conformity has been established for the metal ion dependency of rates of enolization of oxalacetate,[2,4] apparent general acid-catalyzed enolization of oxalacetate,[4] ketonization of enol pyruvate,[3] decarboxylation of oxalacetate,[3,4] and addition of enol pyruvate to pyruvate.[1] It was demonstrated that with use of independently determined intrinsic barriers, rate constants in good agreement with those observed could be calculated from the thermodynamic reaction parameters pertaining to each system. The results of the calculations also provide valuable insight into the nature of the transition states because ΔG° in eq 1 pertains to the *slow* step in a reaction sequence. Although the overall free energy change from reactants to products is path independent, ΔG° for the slow step becomes path dependent for reaction sequences that involve different pre- and postequilibrium steps. This property provides an important tool for the resolution of the proton and metal ion ambiguities that so often plague the mechanistic interpretation of kinetic results. As examples, in metal-ion-catalyzed addition of enol pyruvate to pyruvate,[1] fast reaction rates were indicated to proceed via the formation of a mixed ligand complex in which proton transfer is concerted with carbon–carbon bond formation; apparent general acid-catalyzed enolization of oxalacetate was deduced to proceed via a proton transfer from the $-CH_2-$ group of $-O_2CCOCH_2CO_2H$ to a general base concerted with an intramolecular proton transfer from the 4-CO_2H group to the keto oxygen atom.

The two processes occurring in a concerted reaction require separate reaction coordinates so that with the free energy of the system the progress of the reaction is defined by a surface.[6-13] Recently, in our laboratory a reaction surface based on the Marcus equation has been derived[1] by combining approaches developed by Albery[12] and Guthrie.[3] In the study of enol pyruvate condensation this combined surface was found to successfully reproduce the observed rate constants using the thermodynamic stabilities of the complexes lying at the corners of the surface and an intrinsic barrier that was obtained from metal-ion-independent rates of aldol condensation of acetaldehyde and the retroaldol condensation of 3-penten-2-one hydrate.[1] Similarly, apparent general acid-catalyzed enolization rates of oxalacetate were found to be reproduced by using the appropriate thermodynamic stabilities and an intrinsic barrier obtained from rates of general base-catalyzed enolization.[2] More recently, the combined surface has been found to provide an even better fit[14] to these last data than the model first developed.[2]

Complex-forming metal ions do not appear to alter the intrinsic barrier for a reaction. Nevertheless, metal ions

(1) Cheong, M.; Leussing, D. L. *J. Am. Chem. Soc.* **1989**, *111*, 2541.
(2) Tsai, S.-J.; Leussing, D. L. *Inorg. Chem.* **1987**, *26*, 2620.
(3) Miller, B. M.; Leussing, D. L. *J. Am. Chem. Soc.* **1985**, *107*, 7146.
(4) Leussing, D. L.; Emly, M. *J. Am. Chem. Soc.* **1984**, *106*, 443.
(5) Marcus, R. A. *J. Phys. Chem.* **1968**, *72*, 891; *J. Am. Chem. Soc.* **1969**, *91*, 7224.
(6) Jencks, W. P. *Acc. Chem. Res.* **1976**, *9*, 425.
(7) Jencks, D. A.; Jencks, W. P. *J. Am. Chem. Soc.* **1977**, *99*, 7948.
(8) Jencks, W. P. *Chem. Rev.* **1972**, 705; *Chem. Rev.* **1985**, *85*, 511.
(9) More O'Ferrall, R. A. *J. Chem. Soc. B* **1970**, 274.
(10) Murdoch, J. R. *J. Am. Chem. Soc.* **1983**, *105*, 2660.
(11) Grunwald, E. *J. Am. Chem. Soc.* **1985**, *107*, 125.
(12) Albery, W. J. *J. Chem. Soc., Faraday Trans. 1* **1982**, *78*, 1579; *Ann. Rev. Phys. Chem.* **1980**, *31*, 227.
(13) Guthrie, J. P. *J. Am. Chem. Soc.* **1980**, *102*, 5286. Lamaty, G.; Menut, C. *Pure Appl. Chem.* **1982**, *54*, 1837.
(14) Unpublished results obtained in our laboratory.

0022-3263/90/1955-0666$02.50/0

can induce substantial perturbations of a reaction surface by stabilizing negatively charged species and destabilizing protonated species. These effects can be at least as large as those displayed by substituents on the carbon skeleton of organic molecules. As a further test of the ability of the combined surface to account for the effects of metal ions on reaction rates, investigations are underway regarding general base-catalyzed rates of dissociation of the hydrates and hemiketals of α-keto acids.[15] These reactions exhibit large rate enhancements in the presence of complex-forming metal ions. Prior to an interpretation of these more complicated systems, it was deemed important to establish the applicability of the combined reaction surface to more straightforward metal-ion-free reactions.

A substantial data set has been reported by Sørensen and Jencks[16] for the general base-catalyzed dissociation of hemiacetals and the hydrate of acetaldehyde. The alcohols from which the hemiacetals were formed ranged in acid strength from CF_3CH_2OH ($pK_{a(ROH)}$ = 12.37) to CH_3CH_2OH ($pK_{a(ROH)}$ = 16.1), R = CH_3CH_2, CH_3, CH_3O-CH_2CH_2, $ClCH_2CH_2$, Cl_2CHCH_2, and CF_3CH_2. Base catalysis was observed for H_2O, $RCH_2CO_2^-$ (R = NC, Cl, CH_3O, $ClCH_2$, H), cacodylate, and OH^-. From the dependence of the rates on pK_{ROH} and pK_{HB} it was concluded that the reactions conform to a class n mechanism and are fully concerted with an important degree of proton transfer accompanying carbon–oxygen bond formation in the transition state.[16] It was assumed that in the *vicinity* of the transition state the surface resembles a saddle so that the dependence of log k^B_{diss} on pK_{HB} and pK_{ROH} is described by eq 2.

$$-\log k^B_{diss} = \tfrac{1}{2}p_x \cdot pK_{HB}^2 + \tfrac{1}{2}p_y \cdot pK_{ROH}^2 + p_{xy} \cdot pK_{HB} \cdot pK_{ROH} - \beta_0 \cdot pK_{HB} - \beta^\circ_{1g} \cdot pK_{ROH} + F \quad (2)$$

In fitting the six coefficients of eq 2 to the experimental log k^B_{diss}, it was determined that the rate dependencies observed for seven of the eight base catalysts are consistent with each other but the rates observed for OH^- catalysis are discordant. With the values for the coefficients fitted to the other seven bases, the predicted values of the rate constants for OH^- catalysis are 1.5–2 orders of magnitude lower than the observed values. This discrepancy is clearly evident in Figure 11 of ref 16. Furthermore, it was noted for OH^--catalyzed cleavage that β ($=\delta \log (k^B_{diss}/q)/\delta pK_{HB}$) showed positive deviations from the other values and $\beta_{1g,overall}$ ($=\delta \log (k^B_{diss}/q)/\delta pK_{ROH}$) ranged from −0.7 for the ethyl hemiacetal to −1.5 for the trifluoroethyl hemiacetal. This last value indicates a transition state well off of the reaction surface. It was concluded that a change in mechanism occurred involving little or no protonation of the leaving group in the transition state, at least with the more acidic alcohols.

In the present study we have found that the combined reaction surface quantitatively describes the rate behavior reported by Sørensen and Jencks for all base catalysts *including* OH^- with the adjustment of fewer parameters. The postulated change in mechanism is quite clearly shown in the values of the transition-state coordinates on the reaction surface. The results obtained here are generally in good agreement with those reported earlier, but small, although not insignificant, differences exist.

Reaction Model

In a class n mechanism for general base-catalyzed dissociation of hemiacetals and hydrates the fast preequilibrium removal of the OH proton from the adduct is followed by a concerted general acid-assisted cleavage of the RO–$CH(O^-)$ bond[6,15-19] (Scheme I).

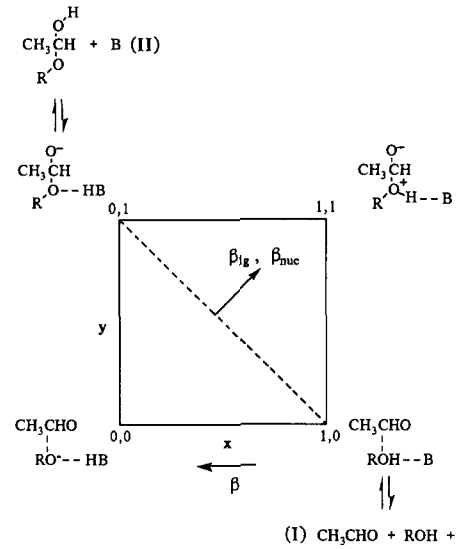

Figure 1. Coordinates for the contour maps for the formation/dissociation of the hydrate and hemiacetals of acetaldehyde.

Scheme I

$$CH_3CH(OH)(OR) + B \rightleftharpoons CH_3CH(O^-)(OR) + HB \text{ (fast)}$$

$$CH_3CH(O^-)(OR) + HB \rightarrow [CH_3CH(O^-)(\cdots OR \cdots H^+ \cdots B)]^\ddagger \rightarrow ROH + CH_3CHO + B \text{ (slow)}$$

Construction of the reaction surface follows the usual practice of first defining the limiting reactions for the slow step.[8,9] These reactions describe the boundaries of the reaction surface. Pertaining to the slow step in Scheme I, the boundary pathways are (i) fast proton transfer from HB to the oxygen atom of the leaving alcohol followed by slow carbon–oxygen bond cleavage:

$$CH_3CH(O^-)(OR) + HB \rightleftharpoons CH_3CH(O^-)(^+HOR) + B \text{ (fast)}$$

$$CH_3CH(O^-)(^+HOR) \rightleftharpoons ROH + CH_3CHO \text{ (slow)}$$

and (ii) slow carbon–oxygen bond cleavage followed by fast proton transfer:

$$CH_3CH(O^-)(OR) \rightleftharpoons CH_3CHO + RO^- \text{ (slow)}$$

$$RO^- + HB \rightleftharpoons ROH + B \text{ (fast)}$$

The coordinate system for contour maps of the reaction surfaces bounded by these reactions is defined in Figure 1. In the direction of association, the reactants, alcohol, aldehyde, and base catalyst, lie at I, and product hemiacetal and base catalyst lie at II. Slow carbon–oxygen bond formation is depicted in the vertical direction of the diagram, and fast transfer of the proton between the base B and the ROH oxygen atom in the horizontal direction. The y coordinate of the contour map is taken as 0 when no carbon–oxygen bond exists and 1.0 when it is fully formed. Similarly, x is 0 when H^+ is not bonded to the RO^- oxygen atom and 1.0 when it is fully bonded. It should be noted that the x axis as defined here is reversed from that as

(15) Kim, Hyo-Soon, unpublished results obtained in our laboratory.
(16) Sørensen, P. E.; Jencks, W. P. *J. Am. Chem. Soc.* **1987**, *109*, 4675.
(17) Funderburke, L. H.; Aldwin, L.; Jencks, W. P. *J. Am. Chem. Soc.* **1978**, *100*, 5444.
(18) McClelland, R. A.; Coe, M. *J. Am. Chem. Soc.* **1983**, *105*, 2718.
(19) Bell, R. P. *The Proton in Chemistry*, 2nd ed.; Cornell University Press: Ithaca, NY, 1973; p 183.

defined in ref 16. In the direction of adduct formation the reactants at I rapidly form a cage complex that lies at the lower right-hand corner (1,0). The immediate product cage complex lies at the upper left-hand coordinate (0,1). Rapid dissociation and proton scrambling yields the final adducts at II. The corners 1,0 and 0,1 define the main reaction diagonal.

Free Energies of the Corner Species

After the boundary reactions have been defined, the next step in constructing the surface is to obtain the free energies of the corner species. If two or more components are involved at a corner, they are assembled into a cage complex. The convention proposed by Albery[12] was employed: the constant for forming a complex between two components is 0.1 M^{-1} if one of them is neutral and 1.0 if one is an H_2O molecule.[20] For charged species the Fuoss equation[21] is used to correct for electrostatic effects, taking the preexponential term as 0.1 M^{-1} to be consistent with the Albery convention.

We have closely followed Sørensen and Jencks[16] with respect to the equilibrium constants for proton transfer and hemiacetal formation, with the modification that Taft equations were set up to facilitate computer calculations. These relationships were developed from the constants reported for the CH_3CH_2OH and CF_3CH_2OH adducts.

Values of $\sigma^*_{R'}$ based on the ionization constants of the alcohols were calculated by rearranging the Ballinger and Long equation[22] for $R'CH_2OH \rightleftharpoons R'CH_2O^- + H^+$:

$$pK_{ROH} = 15.9 - 1.42\sigma^*_{R'} \quad (ROH = R'CH_2OH) \quad (3a)$$

$$\sigma^*_{R'} = (15.9 - pK_{ROH})/1.42 \quad (3b)$$

The proton ionization constants of the hemiacetals, $CH_3CH(OH)(OR) = CH_3CH(O^-)(OR) + H^+$, are defined as pK_4 in ref 16, and this designation is retained here. Values of 13.86 and 13.14 given for the ethyl and trifluoroethyl adducts, respectively, result in the relationship

$$pK_4 = 13.8 - 0.28\sigma^*_{R'} = 13.8 - 0.20(15.9 - pK_{ROH}) \quad (4)$$

pK_3 is defined for the ionization of the zwitterion form of the hemiacetal,[16] $CH_3CH(O^-)(HOR^+) \rightleftharpoons CH_3CH(O^-)(OR) + H^+$. Values of 0.40 and −3.2 cited for the CH_3CH_2OH and CF_3CH_2OH hemiacetals yield

$$pK_3 = 0.26 - 1.38\sigma^*_{R'} = 0.26 - (15.9 - pK_{ROH}) \quad (5)$$

In (5) the ratio 1.38/1.42 = 0.97, which arises when the right hand side of **3b** is substituted for $\sigma^{*\prime}$, has been rounded to 1.0.

Values corresponding to $\log K^\circ_{add}$ for $ROH + CH_3CHO \rightleftharpoons CH_3CH(OH)(OR)$, R = CH_3CH_2- and CF_3CH_2-, are −0.32 and −0.97. From these values

$$\log K^\circ_{add} = -0.345 - 0.25\sigma^*_{R'} = -3.14 + 0.18pK_{ROH} \quad (6)$$

From pK_{ROH} and pK_4, $\log K^-_{add}$ for RO^- addition is calculated to be

$$\log K^-_{add} = 1.68 - 1.37\sigma^*_{R'} = 1.68 - (15.9 - pK_{ROH}) \quad (7)$$

$$RO^- + CH_3CHO \rightleftharpoons CH_3CH(O^-)(OR)$$

The equilibrium constants pertaining to the hydrate were the same as quoted[16] except pK_w was taken as −13.7 to allow for the increased dissociation of H_2O at an ionic strength of 1.0. Consistent with this choice the pK_a of H_2O is 15.4 in units of log M^{-1}. Other values for the hydrate are the statistically corrected $pK_4 = 13.87$, $\log K^-_{add} = 0.21$, and $pK_3 = 1.0$.

Table I. Values of the Cage Formation Constants

(25 °C, I = 1.0)

$\log Q_{00}$ ($CH_3CHO + RO^- + B \rightleftharpoons CH_3CHO\cdots RO^-\cdots B$): −1.82 ($H_2O$), −2.00 ($RCO_2^-cac^-$), −1.00 ($OH^-$)
$\log Q_{01}$ ($CH_3CH(O^-)(OR) + HB \rightleftharpoons CH_3CH(O^-)(OR)\cdots HB$): −0.82 ($H_2O$), −1.00 ($RCO_2^-cac^-$), 0.00 ($OH^-$)
$\log Q_{10}$ ($CH_3CHO + ROH + B \rightleftharpoons CH_3CHO\cdots ROH\cdots B$): −1.00 ($H_2O$), −2.00 ($RCO_2^-$cac, OH^-)
$\log Q_{11}$ ($CH_3CH(O^-)(HOR^+) + B \rightleftharpoons CH_3CH(O^-)(HOR^+)\cdots B$): 0.00 ($H_2O$), −1.00 ($RCO_2^-cac^-$, OH^-)

The free energies assigned to the corner species in Figure 1 relate to the free energies of the dissociated components at I as the zero free energy reference point. These free energies are calculated by using the following relationships in which Q_{ij} represents the formation constant of the cage complex at corner ij:

$$\log K_{10} = \log Q_{10} \quad (8)$$

$$\log K_{11} = pK_3 - pK_{ROH} + \log K^-_{add} + \log Q_{11} \quad (9)$$

$$\log K_{01} = \log K^-_{add} + pK_{HB} - pK_{ROH} + \log Q_{01} \quad (10)$$

$$\log K_{00} = pK_{HB} - pK_{ROH} + \log Q_{00} \quad (11)$$

Values of the cage complex formation constants are given in Table I.

Once the free energies of the corner species are at hand, all that is required to generate a reaction surface and locate the height of the transition state is a value of the intrinsic barrier. In the present case $\Delta G_0^\ddagger$ was not known beforehand, so it became necessary to fit values to the data. The nonlinear curve-fitting program MINUIT[23] was used to minimize $\sum(\log k^B_{diss,obs}/q - \log k^B_{diss,calc}/q)^2$ by locating the "best" value of the intrinsic barrier, or of the parameters in trial-fitting functions which generate $\Delta G_0^\ddagger$. Details of the calculation of $\log k^B_{diss,calc}/q$ for a given value of $\Delta G_0^\ddagger$ are provided in the Appendix.

Examples of generated contour maps are shown in Figure 2. Part A represents the contour map for the addition of ethyl alcohol to acetaldehyde "catalyzed" by H_2O, and part B represents that for the addition of 2-methoxyethanol catalyzed by 2-chloropropionate. The location of each transition state is indicated by an ×. In the region of these transition states the reaction surfaces are seen to be relatively flat, particularly in the direction parallel to the x axis. This feature is typical of these surfaces. Because a search procedure with finite increments of x and y is used rather than an analytical function to find the location of the transition state, the flatness permits the height of the barrier to be obtained with a high degree of precision. The values of x and y contain uncertainties that are of the order of the step size employed in the search. Another potential source of error is the appearance of irregularities in the surface when the transition state lies close to the right-hand axis. The local minima do not differ greatly from the free energy at the global minimum, so reasonably good values of the barrier height are obtained; however, uncertainties of 0.1–0.2 units in $x^\ddagger$ may arise. In this area it is important to ascertain that the true global minimum is located.

The original Guthrie reaction surface[13] exhibits no barrier to proton transfer between the catalyst and alcohol oxygen atoms when their pK_a's become equal as the C–O bond is formed or cleaved. Therefore, the location of the

(20) Taking the cage complex formation constant of H_2O to be 1.0, implies a reference state in which the activity of H_2O is unity. Therefore, in calculation of the formation constants of the corner species the pK_a's of H_3O^+ and OH^- must be taken as 0.0 and 14.0 at I = 0.

(21) Fuoss, R. M. *J. Am. Chem. Soc.* **1958**, *80*, 5059.

(22) Ballinger, P.; Long, F. A. *J. Am. Chem. Soc.* **1960**, *82*, 795.

(23) James, F.; Roos, M. *Comput. Phys. Commun.* **1971**, *14*, 185.

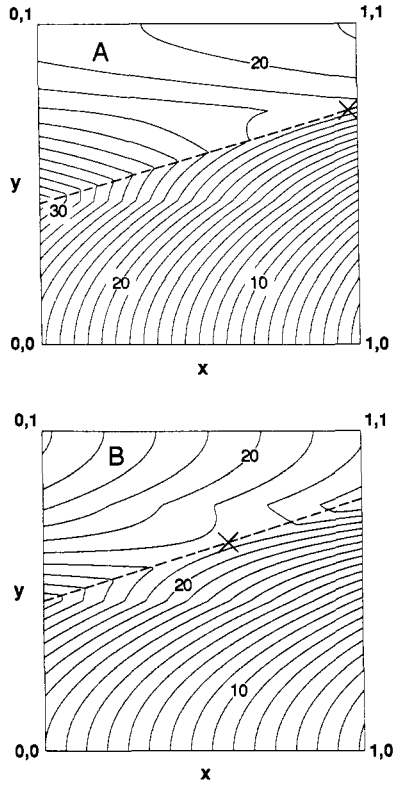

Figure 2. Reaction contour maps for the general base-catalyzed formation and dissociation of hemiacetals of acetaldehyde: (A) ROH = ethanol, B = H_2O; (B) ROH = methoxymethanol, B = chloropropionate. The species at each corner are defined in Figure 1. The transition states are marked by ×. Contours are drawn at intervals of 1 kcal mol^{-1}. The Albery ridges are shown by the dashed lines.

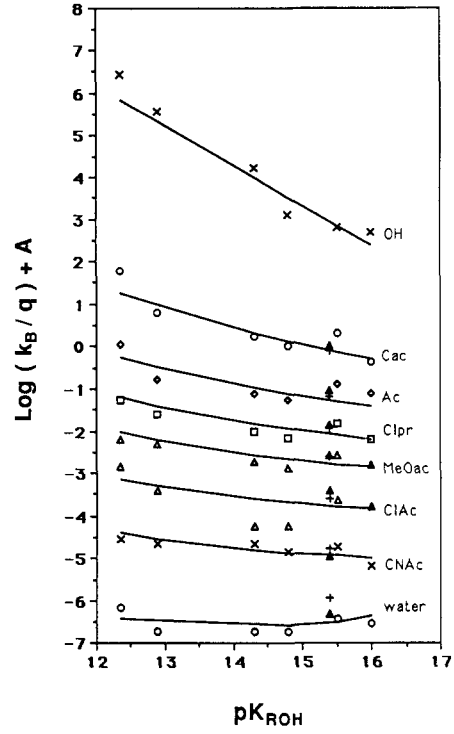

Figure 3. Plot of pK_{ROH} vs the statistically corrected rate constants for the general base-catalyzed dissociation of the hemiacetals and hydrate of acetaldehyde. The solid lines are the theoretical curves for hemiacetal dissociation; (▲) rate constants for the dissociation of the hydrate;[16] (+) calculated rate constants for the dissociation of the hydrate (this work). In the order from H_2O to OH^- the displacements, A, are −2.00, −1.95, −0.95, −0.20, 0.30, 0.80, 1.30, −2.00.

proton in the transition state is ambiguous. This attribute removes the connection between the Brønsted α and β and the transition state coordinates for proton transfer and has recently been challenged.[16] In the contour maps shown in Figure 2, it is seen that the location of the proton in the transition state is defined. The relationship between the coordinates of the transition states and the Brønsted coefficients has been restored and is discussed below in more detail. However, it should be mentioned that removing the ambiguity in the proton location does not answer the original challenge of Sørensen and Jencks, which concerns the effect on the derived surface of the neglect of a barrier for proton transfer. This point is currently under study in our laboratory.

Results

A first attempt at fitting the hemiacetal dissociation rates resulted in the encouraging discovery that with the adjustment of only a single parameter, $\Delta G_0^{\ddagger}$, the combined surface could account with fair accuracy for all of the general base-catalyzed dissociation rates, *including those for OH^- catalysis*. However, a significant improvement in the fit was obtained by assuming that $\Delta G_0^{\ddagger}$ is a linear function of pK_{ROH}. Theoretical curves calculated by using the "best" function

$$\Delta G_0^{\ddagger} = 3.5\ (3) + (0.36\ (3))\mathrm{p}K_{ROH} \qquad (12)$$

are drawn as the solid lines in the plot shown in Figure 3 of log k^{B}_{diss}/q vs pK_{ROH} at constant B. It is seen that quite good agreement between the observed data points and the calculated curves has been obtained over the entire range of base catalysts. $\Delta G_0^{\ddagger}$ ranges from 9.3 kcal mol^{-1} for addition of ethanol to acetaldehyde to 8.0 kcal mol^{-1} for trifluoroethanol addition.

The solid triangles in Figure 3 represent the logarithms of the statistically corrected general base-catalyzed rate constants for dissociation of the hydrate of acetaldehyde. Although these points lie close to the curves for hemiacetal dissociation, they were fitted separately because of the possibility that the value of $\Delta G_0^{\ddagger}$ may not conform to eq 12. The rate constant determined for OH^--promoted dehydration was not included in this analysis because this pathway involves the direct expulsion of OH^- from the adduct or, in the forward direction, nucleophilic attack of OH^- on the keto carbon atom.[16,17] The results of a single parameter fit were satisfactory, yielding a value of 10.4 (2) kcal mol^{-1} for $\Delta G_0^{\ddagger}$, with the standard deviation of a point equal to ±0.22. An intrinsic barrier of 9.0 kcal mol^{-1} is predicted from eq 12. The calculated rate constants are plotted as the crosses in Figure 3. The calculated and observed values are seen to lie in close proximity to each other for all points with the exception of the rates for H_2O catalysis, where the observed value is 0.37 log units smaller than the calculated value. Although this difference is not large, it may signify an additional contribution to the barrier in the proton-transfer step when a very weak base catalyzes the addition of a weak and highly solvated nucleophile.

The intrinsic activation barrier for OH^- attack on the keto carbon is easily evaluated from eq 1 because this reaction involves a single reaction coordinate. With equilibrium constants given above, 1.7×10^4 M^{-1} s^{-1} for the rate constant for OH^--catalyzed dissociation of the hydrate, and values for the precursor and succesor cage complex formation constants listed in Table I, a value of 11.3 kcal mol^{-1} is obtained for the intrinsic barrier. In the present approach the unique character of OH^- reactivity

is seen to be manifested through a relatively high value of $\Delta G_0^{\ddagger}$.

The coefficients of eq 2 were redetermined by using MINUIT. When the eight points for OH^- catalysis were omitted but all others included, the coefficients obtained were essentially the same within their calculated standard deviations as those reported earlier. For the 48-point six-parameter fit the standard deviation, s, was found to be ±0.29. Although a small value of p_x was obtained (p_x = −0.02), the relatively large standard deviation of ±0.07 justifies taking the value as 0.0, as originally reported.[16] For comparison, standard deviations of ±0.27 and ±0.21 were obtained when using the combined surface as a fitting function, respectively, to the dissociation rates of the hemiacetals (48 points, two parameters) and hydrate (7 points, one parameter).

Discussion

It is remarkable that a two-parameter fit using the combined surface is able to account so well for catalysis by all of the bases reported by Sørensen and Jencks for the dissociation of hemiacetals of acetaldehyde.[16] In view of the failure of the earlier model to account for OH^- catalysis, it is gratifying to find that these data are readily accommodated in the present treatment. The calculated curves shown in Figure 3 for a plot of log k^B_{diss}/q vs pK_{ROH} show that the data points have been fitted over the entire range of catalyst basicities from H_2O to OH^-, and the change in slope with varying pK_{HB} is also reproduced. Conformance to a class n mechanism for most of the reactions is verified, as is also the earlier conclusion that H_2O serves as a typical general base catalyst. It is not necessary to invoke a unique cyclic mechanism for H_2O catalysis.[16] Support is also provided the conclusion that OH^--catalyzed hydration involves direct nucleophilic attack on the unsaturated carbon atom of acetaldehyde, or expulsion of OH^- from the hemiacetal in the reverse direction. As nucleophiles, H_2O and OH^- behave differently from the alcohols in the sense that they exhibit higher intrinsic barriers toward addition to an unsaturated carbon atom.

In view of the adjustment of six parameters in the fit of the saddle surface to the data, it is not surprising that a comparison of the theoretical curves drawn in Figure 11 of ref 16 with those of Figure 3 in this paper reveals that the combined surface yields somewhat flatter theoretical curves. With both models, rates observed for dissociation of the trifluoroethanol hemiacetals tend to be faster than those predicted. The combined surface furnishes predictions, with good accuracy, of the rates for base catalysis by H_2O through chloropropionate, but the rates for the more basic catalysts tend to be underestimated. The saddle model performs better in the range cyanoacetate through acetate but also yields low estimates of the rates obtained for cacodylate and OH^-. Although the combined surface is able to accommodate to a wider variation in catalyst basicity, the saddle surface provides a better description of the rate–catalyst dependency over a limited range of catalyst basicities.

Values of $\Delta G_0^{\ddagger}$ for nucleophilic attack on the aldehyde carbon atom or for dissociation of the adduct, decrease in the order $OH^- > H_2O > CH_3CH_2O^- > CH_3O^- > CH_3OCH_2CH_2O^- > CH_2ClCH_2O^- > CHCl_2CH_2O^- > CF_3CH_2O^-$. With the alcohols this order is determined by eq 12. Because the quadratic term in the Marcus equation is small for these reactions, the height of the calculated activation barrier tends to display a direct linear dependence on the intrinsic barrier. Therefore, an increase in $\Delta G_0^{\ddagger}$ with increasing pK_{ROH} results in a tendency for rates to decrease in this same order, although this effect is modified by accompanying changes in thermodynamic stabilities of the corner species.

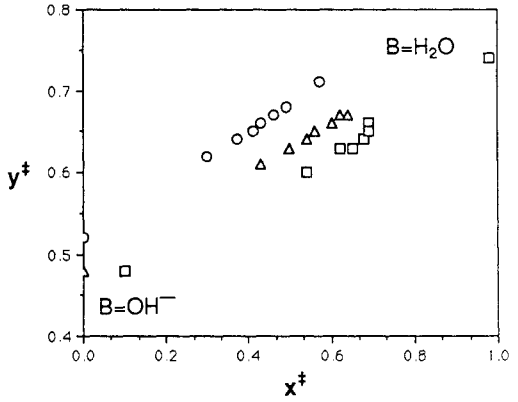

Figure 4. Calculated transition-state locations for the general base-catalyzed addition of alcohols to acetaldehyde: (○) CF_3CH_2OH; (△) $MeOCH_2CH_2OH$; (□) CH_3CH_2OH.

There is precedence for an inverse component of nucleophile basicity on reaction rates.[24] In hydroxylic solvents rates of nucleophilic attack of highly basic nucleophiles on substrates may be found to exhibit a smaller dependence on σ than rates of attack of weakly basic nucleophiles.[25] In some cases rates may even decrease as nucleophilic basicity increases.[26] The phenomenon is attributed to the combined effects of an increase in solvational energy as nucleophile basicity increases and the necessity of a nucleophile to undergo partial desolvation to make available an electron pair for bond formation to an electrophile.[24] The energy required for desolvation contributes to the height of the energy barrier that a reaction must cross. The small value found for the first term on the right-hand side of eq 12 implies that desolvation contributes substantially to the reaction barrier. The relatively high barriers noted for OH^- and H_2O addition are consistent with this picture. These nucleophiles have high solvational energies owing to extensive hydrogen bonding to surrounding solvent and to their excellent fit into the solvent structure.

The coordinates of the transition states obtained from the calculations for the formation/dissociation of the ethanol, methoxyethanol, and trifluoroethanol hemiacetals are plotted in Figure 4. Catalysis by OH^- is represented by the leftmost point in each series, and H_2O catalysis by the rightmost point. These results support the conclusions drawn by Sørensen and Jencks that most of the processes are concerted.[16] However, at the one extreme of H_2O-catalyzed addition of CH_3CH_2OH to acetaldehyde (the weakest base catalyst and the most weakly acidic alcohol) the transition state is calculated to lie close to the right-hand axis ($x^{\ddagger}$ = 1.0), indicating that little proton transfer from alcohol to solvent occurs in the transition state. At the other extreme of catalysis by OH^- of the addition of CF_3CH_2OH (the strongest base and the most acidic alcohol) the transition state is calculated to lie near the left-hand axis ($x^{\ddagger}$ = 0.0), indicating that the pathway essentially involves the direct addition of RO^- to acetaldehyde, as concluded earlier.[16] Dissociation of the ethyl hemiacetal may also involve slight assistance from proton transfer from H_2O. Thus, $x^{\ddagger}$ ranges from approximately 0 on one

(24) Jencks, W. P. In *Nucleophilicity*; in Advances in Chemistry Series, No. 215, Harris, J. M., McManus, S. P., Eds.; American Chemical Society: Washington, DC, 1987; Chapter 10.
(25) Richard, J. P.; Jencks, W. P. *J. Am. Chem. Soc.* **1984**, *106*, 1373.
(26) Jencks, W. P.; Haber, M. T.; Herschlag, D.; Nazaretian, K. L. *J. Am. Chem. Soc.* **1986**, *108*, 479.

Table II. Comparison of β and $\beta_{lg,overall}$ Obtained by Fitting the Combined Surface and Saddle Surface Models to Representative Dehydration and Hemiacetal Dissociation Rate Data Reported in Ref 16

		β			$\beta_{lg,overall}$		
pK_{ROH}	pK_{HB}	ref 16[a]	this work	calc[b]	ref 16[c]	this work	calc[d]
16.0	2.23	0.41	0.28	0.31	0.21	−0.06	−0.10
	3.93	0.41	0.35	0.35	0.10	−0.15	−0.16
	6.16	0.41	0.45	0.46	−0.06	−0.25	−0.30
14.30	2.23	0.53	0.38	0.38	−0.13	−0.16	−0.15
	3.93	0.53	0.46	0.46	−0.25	−0.26	−0.30
	6.16	0.53	0.57	0.57	−0.40	−0.38	−0.40
12.37	2.23	0.66	0.52	0.51	−0.52	−0.30	−0.23
	3.93	0.66	0.60	0.59	−0.64	−0.41	−0.38
	6.16	0.66	0.70	0.70	−0.79	−0.52	−0.52

[a] Eq 14. [b] $\beta_{calc} = 1 - x^{\ddagger}$. [c] Eq 13. [d] $\beta_{lg,overall\,calc} = x^{\ddagger} + y^{\ddagger} - 1.44$.

side of the surface to 1 on the other side. Jencks has stressed that the saddle surface is valid only for small excursions of the transition state on the reaction surface[7,8,16] and attributed the breakdown with OH^- catalysis to failure of this condition. In contrast, the combined surface is seen to provide values of rate constants consistent with the observed values over wide ranging changes in the locations of the transition states.

The shifts in the location of the transition states as pK_{HB} and pK_{ROH} are varied are somewhat complicated. Transition states that lie on the vertical axes exhibit a Hammond effect under the influence of a perturbation, i.e., the transition state is shifted away from the corner that becomes relatively more stable. An increase in pK_{ROH}, for example, brings about an increase in the stability of corner 1,1 and a decrease in the stability of corner 0,0. These changes essentially effect a rotation about the main diagonal. Transition states that lie on either of the vertical axes shift in the direction of smaller $y^{\ddagger}$. In the middle of the contour map, however, an increase in pK_{ROH} at constant HB causes $x^{\ddagger}$ to increase, an anti-Hammond effect, and $y^{\ddagger}$ to decrease slightly, a Hammond effect. An increase in pK_{HB} at constant ROH causes the free energies along the left-hand vertical axis to become more negative. Transition states lying on either axis are not influenced by this change, but in the middle of the map both $x^{\ddagger}$ and $y^{\ddagger}$ decrease, an anti-Hammond effect.

The saddle surface and the combined surface comprise entirely different types of functions with which to fit the data. Of interest is a comparison of the Brønsted coefficients obtained with the two models. Because derivatives are being considered, differences between the saddle surface and combined surface will be emphasized. Analytical functions giving the Brønsted parameters are not readily available using the combined surface, so to obtain values of β and $\beta_{lg,overall}$ quadratic polynomials were fit to the calculated log k^{B}_{diss}/q, and these polynomials were appropriately differentiated. The quality of the fit was quite good with the standard deviation of a point being about 0.005 log units. Values obtained from the saddle surface were calculated by using the reported[16] analytical functions expressed in eq 13 and 14. The results are summarized in Table II.

$$\beta_{lg,overall} = 0.2pK_{ROH} - 0.07pK_{HB} - 2.83 \quad (13)$$

$$\beta = -0.07pK_{ROH} + 1.53 \quad (14)$$

Sørensen and Jencks report[16] that β is dependent only on pK_{ROH}, but the results obtained here indicate a small additional dependency on pK_{HB} with values of $\delta \log \beta/\delta pK_{HB}$ falling in the range 0.04–0.05. This dependency does not signify drastic differences between the results obtained with the two surfaces because β values obtained with the combined surface bracket the values obtained with the saddle surface. The combined surface yields a smaller spread in the $\beta_{lg,overall}$ but once again the trends shown by the two models are the same and no major differences are shown. Reflecting this smaller change, p_y ($=-\delta\beta_{lg,overall}/\delta pK_{ROH}$) is found here to be about −0.07, in contrast to −0.20 reported earlier.[16] On the other hand, the cross coefficient p_{xy} ($=-\delta\beta/\delta pK_{ROH}$) is found here to be 0.068, in excellent agreement with 0.074 reported earlier.

Brønsted coefficients are considered to provide clues regarding the location of transition states on a reaction surface. Because the reaction coordinates are also determined in the calculations performed with the combined surface, it was deemed worthwhile to examine the correlation between these parameters.

β represents a displacement from the right-hand vertical axis of the coordinate system defined in Figure 1:

$$\beta = 1 - x^{\ddagger} \quad (15)$$

In comparing the results obtained here with those reported by Jencks and co-workers,[6-8,16,17] it should be noted that the reversal in the x axis causes β, as defined in Figure 1 of this work, to increase from right to left, whereas a definition giving an increase in the opposite direction is used by Jencks, e.g., as shown in Figure 2A of ref 7.

$\beta_{lg,overall}$ describes the dependence of the rate of general base-catalyzed splitting of alcohol from hemiacetal on the pK_a of ROH: $\beta_{lg,overall} = \delta \log(k^{B}_{diss}/q)/\delta pK_{ROH}$. A change in pK_{ROH} affects the rate in several ways: through its influence on the ionization of the hemiacetal ROCOH proton, through the ease with which the RO–CO^- bond is split, and through the affinity of the departing oxygen atom for the proton offered by the conjugate acid of the apparent general base catalyst. It is convenient to cast the discussion in terms of k^{B}_{add}, which is directly related to the coordinates of the transition state on the reaction surface:

$$k^{B}_{diss}/q = k^{B}_{add}/qK^{\circ}_{add} \quad (16)$$

$$\beta_{lg,overall} = \delta \log (k^{B}_{add}/q)/\delta pK_{ROH} - \delta \log K^{\circ}_{add}/\delta pK_{ROH} \quad (17a)$$

$$= \beta_{nuc} - \delta \log K^{\circ}_{add}/\delta pK_{ROH} \quad (17b)$$

K°_{add} is the equilibrium constant given by eq 6. In the coordinate system defined in Figure 1, β_{nuc} ($=\delta \log (k^{B}_{add}/q)/\delta pK_{ROH}$) is measured from the main reaction diagonal in the direction parallel to the off-diagonal axis. Values range from +1.0 to −1.0, with 0 lying on the main reaction diagonal. β_{lg} for the splitting of the alcohol from the ionized hemiacetal lying at corner 0,1 is equal to β_{nuc}.[7] In terms of the transition state coordinates[7]

$$\beta_{lg} = \beta_{nuc} = x^{\ddagger} + y^{\ddagger} - 1 \quad (18)$$

Substitution of (18) into eq 17b yields the result

$$\beta_{1g,overall} = x^{\ddagger} + y^{\ddagger} - 1 - \delta \log K^{\circ}_{add}/\delta pK_{ROH} \quad (19)$$

From eq 6, $\delta \log K^{\circ}_{add}/\delta pK_{ROH} = 0.18$. Therefore

$$\beta_{1g,overall} = x^{\ddagger} + y^{\ddagger} - 1 - 0.18 = x^{\ddagger} + y^{\ddagger} - 1.18 \quad (20)$$

When values of $\beta_{1g,overall}$ calculated from eq 20 by using the transition-state coordinates with the combined surface were compared with those calculated by differentiating the polynomials fitted to the log $k^{B}_{diss,calc}/q$, it was observed that the former were uniformly higher than the latter by 0.26 units. this displacement is exactly equal to $(\delta\Delta G_0^{\ddagger}/\delta pK_{ROH})/1.36 = 0.36/1.36 = 0.26$, as given by differentiation of eq 12, and implies a relationship having the form

$$\beta_{1g,overall} = x^{\ddagger} + y^{\ddagger} - 1 - \delta \log K^{\circ}_{add}/\delta pK_{ROH} - (\delta\Delta G_0^{\ddagger}/\delta pK_{ROH})/1.36 \quad (21)$$

or for the present case

$$\beta_{1g,overall} = x^{\ddagger} + y^{\ddagger} - 1.44 \quad (22)$$

The requirement for a term expressing the dependence of $\beta_{1g,overall}$ on $\delta\Delta G_0^{\ddagger}/\delta pK_{ROH}$ is not surprising in view of the relatively small dependence noted for the calculated transition-state coordinates on small changes in $\Delta G_0^{\ddagger}$. These changes, however, directly affect the logarithms of the calculated rate constants and must be included in equations that relate β_{1g} and $\beta_{1g,overall}$ to the transition-state coordinates.

Equations 21 and 22 illustrate the important point that a value found for a Brønsted coefficient may reflect not only the coordinates of the transition state but also any dependence that the intrinsic barrier has on the reaction variable pertaining to that coefficient. Unless this dependence is known, deductions regarding the transition-state location are uncertain. However, once this dependence is known, the Brønsted coefficients may be accurately calculated from the reaction coordinates and vice versa. In Table II it is seen that theoretical values of the Brønsted coefficients calculated by using eq 22 are in very good agreement with the values calculated by differentiating polynomials that had been fitted to the log $k^{B}_{diss,calc}/q$.

Qualitatively, the shift of the transition state to the left in Figure 4 as pK_{HB} increases is consistent with the positive value of $\delta\beta/\delta pK_{HB}$ that is predicted by using the combined surface to model the system. An accompanying decrease in $y^{\ddagger}$ indicates that in the direction of addition, bond making between the alcohol oxygen atom and the aldehyde carbon atom occurs earlier along the reaction coordinate. The decrease in the sum of $x^{\ddagger}$ and $y^{\ddagger}$ is manifested as a decrease in β_{1g}. At constant HB, as pK_{ROH} becomes smaller, $x^{\ddagger}$ decreases while $y^{\ddagger}$ increases. This causes the transition state to shift toward the upper left-hand corner. Carbon–oxygen bond making becomes more advanced in the transition state, and the aldehyde moiety becomes more negatively charged. Because the shifts along the $y^{\ddagger}$ axis are smaller than those along the $x^{\ddagger}$ axis, β_{1g} is predicted to become less positive, as is shown in the results given in Table II.

These changes in transition state are in generally good agreement with the extent of C–O bond cleavage as deduced from studies of secondary isotope effects on hemiacetal dissociation. Palmer and Jencks[27] have examined the effects of α-deuterium substitution on rates of dissociation of formaldehyde hemiacetals. Ratios of k_{2H}/k_{2D} were found to increase in the order of increasing basicity of the catalyst, H_2O < acetate < OH^-, demonstrating that C–O bond breaking in the transition state increases as the catalyst basicity increases. In Figure 4 the extent of bond cleavage in the direction of dissociation is measured by the difference $1 - y^{\ddagger}$. In full accord with the observed isotope effect, values of $y^{\ddagger}$ are seen to decrease ($1 - y^{\ddagger}$ to increase) markedly as the basicity of the general base catalyst increases. Palmer and Jencks[27] also deduced that as ROH becomes more basic, there is a larger movement of the proton than of the electrophile toward the alcohol. This deduction is quite clearly supported in Figure 4 by the large changes in $x^{\ddagger}$ relative to small changes in $y^{\ddagger}$. Unexplained, however, are the ratios 1.23, 1.28, and 1.34 determined for the α-isotope effect on acetate-catalyzed dissociation of the ethyl, chloroethyl, and trifluoroethyl hemiacetals of formaldehyde, respectively. These ratios indicate a tendency for $1 - y^{\ddagger}$ to increase as pK_{ROH} becomes smaller when catalysts in the midrange of basicity are employed. It is seen in Figure 4 that the $y^{\ddagger}$ values tend to become slightly larger as pK_{ROH} decreases, denoting changes in C–O bond breaking in the opposite direction than are shown by the isotope effects. At least part of this discrepancy seems to reflect inherent differences between the formaldehyde and acetaldehyde systems. A brief examination of the formaldehyde rates[17] using the combined surface reveals that $y^{\ddagger}$ is essentially unchanged at 0.59 for the dissociation of the ethanol and trifluoroethanol hemiacetals of formaldehyde, although the respective values of $x^{\ddagger}$, which are 0.60 and 0.43, change appreciably.[28] This change in the relationship between $y^{\ddagger}$ and pK_{ROH} is in the correct direction, but the combined surface is seen once more to fail to provide a highly accurate description of the behavior of these systems when catalysts in the midrange of basicities are employed.

In summary, the dissociation of acetaldehyde hemiacetals constitutes a third example of a reaction system that satisfactorily conforms to the combined reaction surface. With the adjustment of relatively few parameters, this reaction surface accounts for the major observations reported for the dissociation of acetaldehyde hemiacetals over the full range of base catalysts available in aqueous systems, although sensitivity is lacking with respect to describing the finer features of the reaction systems. By separating the effects of thermodynamics on the reaction rates from the effects of kinetics (which are reflected in the values of the intrinsic barriers), the model aids in gaining useful insight into mechanistic features that might otherwise escape notice or be difficult to resolve. Further refinements of the model are in progress.

Appendix: Construction of the Combined Reaction Surface

In a reaction that proceeds along the single reaction coordinate y, the free energy of the reactants as a function of displacement along the coordinate is approximated by the parabolic function (centered at $y = 0$)

$$\Delta G_{reactants} = 4\Delta G_0^{\ddagger} y^2 + \Delta G^{\circ}_{reactants} \quad (A1)$$

The free energy of the products is given by the parabolic function (centered at $y = 1$)

$$\Delta G_{products} = 4\Delta G_0^{\ddagger}(1 - y)^2 + \Delta G^{\circ}_{products} \quad (A2)$$

Equation 1 with $\Delta G^{\circ} = \Delta G^{\circ}_{products} - \Delta G^{\circ}_{reactants}$ gives the height of the barrier with respect to $\Delta G^{\circ}_{reactants}$ at the

(27) Palmer, J. L.; Jencks, W. P. *J. Am. Chem. Soc.* **1980**, *102*, 6472.

(28) The intrinsic barriers for formaldehyde hemiacetal dissociation are lower and show a smaller dependence on pK_{ROH} than those of acetaldehyde. The values are −7.2 and −7.8 kcal mol^{-1} for the trifluoroethanol and ethanol hemiacetals, respectively.

intersection of the reactant and product parabolas, the transition state.

The coordinate for the intersection is

$$y^{\ddagger} = (4\Delta G_0^{\ddagger} + \Delta G^{\circ})/8\Delta G_0^{\ddagger} \quad \text{(A3)}$$

To calculate the free energy–reaction coordinate profile for a reaction proceeding from $y = 0$ to $y = 1.0$, eq A1 is used in the region $y \leq y^{\ddagger}$ and eq A2 is used in the region $y > y^{\ddagger}$.

A surface for a two reaction coordinate system is obtained by extending the construction of the single reaction coordinate profile at intervals along the second reaction coordinate. If the reaction that has been chosen to proceed along the x axis is inherently fast, such as proton transfer between oxygen atoms, its barrier is assumed to be negligible, and the free energies along the x axis are obtained by using a linear interpolation of the free energies of the corner species:

$$\Delta G^{\circ}_{x0} = (1 - x)\Delta G^{\circ}_{00} + x\Delta G^{\circ}_{10}, \quad \text{when } y = 0 \quad \text{(A4)}$$

$$\Delta G^{\circ}_{x1} = (1 - x)\Delta G^{\circ}_{01} + x\Delta G^{\circ}_{11}, \quad \text{when } y = 1 \quad \text{(A5)}$$

If $\Delta G_0^{\ddagger}$ for the process occurring parallel to the y axis is known (or a value has been assumed), the values of $y^{\ddagger}$ for the free energy maximum that lies on the profile corresponding to a given value of x is located by using eq A3 with

$$\Delta G^{\circ} = \Delta G^{\circ}_{x1} - \Delta G^{\circ}_{x0} \quad \text{(A6)}$$

At a given value of x, a vertical reaction profile is constructed as described above for the case of a single reaction coordinate with the modifications that in eq A1 and A2, $\Delta G^{\circ}_{\text{reactants}}$ is given by eq A4. $\Delta G^{\circ}_{\text{products}}$ by eq A5, and ΔG° by eq A6. A family of profiles is constructed from $x = 0$ to $x = 1$ at chosen increments of x to give a network of ΔG_{xy} values.

This process generates the Albery component of the reaction surface. It is characterized by a ridge that joins the two maxima that fall on the vertical axes.[12] The Albery ridges are shown as the dashed lines in Figure 2.

The Guthrie component is generated by calculating only the vertical profiles at $x = 0$ and $x = 1.0$. The interior points are filled in at given intervals of y by using eq A7 to linearly interpolate in the horizontal direction.

$$\Delta G_{xy} = (1 - x)\Delta G_{0y} + x\Delta G_{1y} \quad \text{(A7)}$$

When the free energies of the corner species bear the appropriate relationships to each other, the Guthrie surface develops a horizontal contour that falls between the two maxima lying on the vertical axes. This "catalytic" contour provides a relatively low and constant free energy route by which the reaction system may traverse from the reactant side to the product side and avoid both of the maxima that lie on the vertical axes.

This derivation of a Guthrie surface differs from that originally presented[13] to make it consistent with eq 1.

The combined surface is obtained by averaging the values calculated for each pair of ΔG_{xy}. In this way the interior of the surface is generated from the properties of the four edges by interpolation in both the x and y directions.

In practice a full surface need not be constructed to obtain the barrier height and location. Inspection of several sets of curves for the present set of reactions indicates that the transition state lies either on or close to the Albery ridge. The value of y_{ridge} is equal to the value of $y^{\ddagger}$ that corresponds to a given value of x. In a computer search for the transition state, values of free energy are calculated only in the vicinity of the Albery ridge. Computations are performed from $x = 0$ to $x = 1$ at chosen increments of x. At each x, y_{ridge} is evaluated. Starting at a value of y slightly smaller than y_{ridge} and holding x constant, successive values of the averaged ΔG_{xy} are obtained at given intervals of y until the value passes through a maximum. The free energy at this maximum and the coordinates are stored, x is incremented, and the entire process is repeated. After the surface has been traversed, the smallest of these maximum averaged ΔG_{xy} is found and taken as the height of the reaction barrier, $\Delta G^{\ddagger}$, relative to the reference state. The corresponding coordinates provide the location of the transition state.

For the final computations increments of x and y equal to 0.01 were employed. A finite mesh introduces some uncertainty in locating the transition state, but because the surface is relatively flat in this region errors in the height of the energy barrier are negligible.

In the present calculations the free energy of the unassociated components (at I in Figure 1) was taken as reference zero free energy. The rate constant for addition is calculated from the barrier obtained above:

$$\log k^{\text{B}}_{\text{add}}/q = -(\Delta G^{\ddagger} - 17.4)/1.36 \quad \text{(A8)}$$

and the rate constant for dissociation is calculated from

$$\log k^{\text{B}}_{\text{diss}}/q = \log k^{\text{B}}_{\text{add}}/q - \log K^{\circ}_{\text{add}} \quad \text{(A9)}$$

Registry No. $H_3CCH(OH)OEt$, 7518-70-9; $H_3CCH(OH)OMe$, 563-64-4; $H_3CCH(OH)OCH_2CH_2OCH_3$, 108743-21-1; $H_3CCH(OH)OCH_2CH_2Cl$, 108743-22-2; $H_3CCH(OH)OCH_2CHCl_2$, 108743-23-3; $H_3CCH(OH)OCH_2CF_3$, 54872-49-0; H_2O, 7732-18-5; $NCCH_2CO_2^-$, 23297-32-7; $ClCH_2CO_2^-$, 14526-03-5; $MeOCH_2CO_2^-$, 20758-58-1; $ClCH_2CH_2CO_2^-$, 5102-76-1; $CH_3CO_2^-$, 71-50-1; $Me_2AsO_2^-$, 15132-04-4; OH^-, 14280-30-9; $CH_3CH(OH)OH$, 4433-56-1.